Absolute calibration of single-photon and multiplexed photon-number-resolving detectors

Lior Cohen,[1] Yehuda Pilnyak,[1] Daniel Istrati,[1] Nicholas M. Studer,[2] Jonathan P. Dowling,[2,3,4] and Hagai S. Eisenberg[1,*]

[1]*Racah Institute of Physics, Hebrew University of Jerusalem, Jerusalem 91904, Israel*

[2]*Hearne Institute for Theoretical Physics, and Department of Physics and Astronomy, Louisiana State University, Baton Rouge, Louisiana 70776, United States*

[3]*NYU-ECNU Institute of Physics at NYU Shanghai, 3663 Zhongshan Road North, Shanghai, 200062, China*

[4]*2CAS-Alibaba Quantum Computing Laboratory, CAS Center for Excellence in Quantum Information and Quantum Physics, University of Science and Technology of China, Shanghai 201315, China*

(Received 19 December 2017; published 5 July 2018)

Single-photon detectors are widely used in modern quantum optics experiments and applications. Like all detectors, it is important for these devices to be accurately calibrated. A single-photon detector is calibrated by determining its detection efficiency; the common method to measure this quantity requires comparison to another detector. Here, we suggest a method to measure the detection efficiency of a single-photon detector without requiring an external reference detector. Our method is valid for individual single-photon detectors as well as multiplexed detectors, which are known to be photon number resolving. The method exploits the even-number photon-statistics of a nonlinear source, as well as the nonlinear loss of a single-photon detector that occurs when multiple photons are incident simultaneously. We have analytically modeled multiplexed detectors and used the results to experimentally demonstrate the calibration of a single-photon detector without the need for an external reference detector.

DOI: 10.1103/PhysRevA.98.013811

I. INTRODUCTION

Information about the photon number is required for applications in many diverse fields such as linear-optical quantum computing [1,2], superresolution [3], supersensitive microscopy [4], foundations of quantum mechanics [5], and quantum key distribution [6]. To date, there are a few techniques to measure photon-number [7]. One leading approach is to use single-photon detectors (SPDs), either with splitters to separate photons into different SPDs (spatial multiplexing) or as an array of SPDs [8]. It is also known that one SPD can be used if the splitters separate the photons into different time slots (time multiplexing) [9]. The signal from all SPDs is summed yielding the photon-number information. Though providing this information, these multiplexing techniques are not considered as full photon-number-resolving (PNR) detectors due to saturation of the elements [10]. We use "multiplexing PNR detectors" as a general name for time multiplexing, spatial multiplexing and array of SPDs throughout this paper.

To have precise photon number information of the measured quantum state, the detector must be characterized, and in particular its detection efficiency must be measured. Characterization of the detection efficiency is here considered to be calibration of the device. The common procedure to calibrate SPDs is to use correlated photon pairs from a twin-beam state. This method was first suggested in 1977 by Klyshko [11] and demonstrated experimentally two years later [12]. Two detectors are required for this method because the coincidence rate must be known to calculate the efficiencies. Recently, the coincidence method was adapted to PNR detectors [13–16].

There are other methods to calibrate the detection efficiency [17–20]. One such method utilizes a single SPD, which is time-multiplexed to temporally separate the incident photons [17]. Then, the detection efficiency is found as in the coincidence method. Though technically Chen *et. al.* demonstrated calibration with a single SPD, practically they calibrated by coincidence counts, a measurement which requires more than one detector or more than one detection time slot. Here, we develop a model to characterize a multiplexing PNR detector, and apply the analysis to calibration of a single SPD. Using the photon statistics of the single-mode and two-mode squeezed vacuum states (SMSV and TMSV, respectively) [21], we show how the detection efficiency is found by the single counts only, without coincidence counts as used in previous methods.

This paper is arranged as follows. A model for a general multiplexing PNR detector is presented in Sec. II. In Sec. III we limit the discussion to one SPD and show how the efficiency can be measured using SMSV and TMSV light. The setup to perform this calibration is also described there. Results of the calibration procedures are presented in Sec. IV. There we also compare between the use of SMSV and TMSV for the calibration.

II. CHARACTERIZATION MODEL

Given a multiplexing PNR detector, there is a problem with counting the photon number due to several internal effects distorting the measurement statistics [22]. The incident photon statistics can, however, be reconstructed if the distortion effects are well quantified. We consider several detection parameters:

*Corresponding author: hagai.eisenberg@mail.huji.ac.il

efficiency, number of SPD elements (finite detector size), dark count rate, and cross-talk rate. To date, there lacks an analytical model for all of these effects. In particular, the combined effects of finite-size with cross-talk are not well known [23]. Now, we present an analytical model which incorporates all of these effects.

A. Loss

When a photon hits the detector, there is a nonzero probability that either the avalanche process will not start or will stop before a detection occurs [24]. This is an intrinsic property of any realistic device, but can also be attributed to inefficient light coupling to the device. In such a scenario the photon is considered lost. The detection efficiency is then defined as the probability for detecting a single-photon. We assume the detection efficiency is uniform for all SPD elements and is denoted by η. If n photons hit the detector, the probability for m elements to be activated is given by a binomial distribution [22]

$$M^{\eta}_{\text{loss}}(m,n) = \binom{n}{m}\eta^m(1-\eta)^{n-m}, \tag{1}$$

where $\binom{n}{m} = \frac{n!}{m!(n-m)!}$ for $n \geqslant m \geqslant 0$ or zero otherwise. Here we assume each photon hits a different element. This assumption is not valid in general but will be later corrected for by including the effects of finite detector size.

B. Finite-size

Each individual element of the multiplexing PNR detector is an SPD. As such, the signal from each element does not depend on the number of photons hitting it. Therefore, if more than one photon hits an element, only one can be detected, causing a nonlinear loss of photons and a distortion of the incident photon statistics. The probability for m photons to hit k different elements at an N-element detector, is [25]

$$M^{N}_{FS}(k,m) = \frac{1}{N^m}\binom{N}{k}k!S(m,k), \tag{2}$$

where $S(m,k) = \frac{1}{k!}\sum_{j=0}^{k}(-1)^{k-j}\binom{k}{j}j^m$ are known as the Stirling numbers of the second kind [26].

C. Dark-counts

After k elements fire due to photon detections, there are still $(N-k)$ elements which are free to be activated due to a dark-count: a false event without a photon hit. This is typically due to thermal electrons. We assume that each element has equal probability d for this event to occur. If p is the total number of elements that fire, including those elements which report a dark count, then $p-k$ is the number of elements that fire due to a dark count event. The probability for $(p-k)$ elements to be activated due to dark-counts where $(N-k)$ elements are available is

$$M^{d}_{\text{DC}}(p,k) = \binom{N-k}{p-k}d^{p-k}(1-d)^{N-p}. \tag{3}$$

D. Cross-talk

Cross-talk is an effect where a recombination of an electron and a hole generates a photon and this photon is detected in a nonactivated neighbor element [27]. All multiplexing PNR detectors suffer from this effect, but it is not relevant when the SPDs are distant and the cross-talk counts can be temporally filtered. Where the detector is an SPD array, the cross-talk counts cannot be filtered and the cross-talk effect is relevant. Cross-talk is most likely to happen at nearest-neighbor elements and we neglect other scenarios.

Up to date, a few cross-talk models are available [22,28–30]. Each has its own advantages and disadvantages, but none of them takes into account the finite size of the detector. Thus, we introduce an alternative model for the cross-talk. Until this point, uniformity was the only assumption. Yet, to solve analytically the cross-talk effect, more assumptions must be made. The probability of cross-talk strongly depends on the number of nonactivated neighbors, but it is impossible to know how many nearest neighbors are available. Instead, we check how many nearest neighbors are available on average, where p elements already have been activated, and this number is plugged in as the total effective number of nearest neighbors, $\text{ENN} = 4(1-\frac{p}{N})\frac{N-\sqrt{N}}{N-1}$. This linearly dependent formula is reasonable as it is zero if all elements are not available ($p = N$). On the other limit, if all elements are available the ENN nears four, a limit imposed by the rectangular detector's edge. This formula was derived simply by randomly choosing p elements and counting their nearest neighbors, and then averaging many different configurations.

Let us define x as the probability for cross-talk to one of the available nearest neighbors. By assuming $x \ll 1$, terms proportional to higher powers of x are neglected, in particular, cross-talk generated by another cross-talk and more than one cross-talk event per element. Thus, the probability for one element to generate a cross-talk event to any available nearest neighbors is $4x(1-\frac{p}{N})\frac{N-\sqrt{N}}{N-1}$ and for p elements to generate ℓ cross-talk events is just a binomial combination. Thus, under the mentioned assumptions, the probability for $(s-p)$ elements to be activated by cross-talks from p elements is

$$M^{\tilde{x}}_{XT}(s,p) = \binom{p}{s-p}\left[\tilde{x}\left(1-\frac{p}{N}\right)\right]^{s-p} \times \left[1-\tilde{x}\left(1-\frac{p}{N}\right)\right]^{2p-s}, \tag{4}$$

where we define $\tilde{x} = 4x\frac{N-\sqrt{N}}{N-1}$.

E. Detected probabilities

The real photon number probabilities ($\vec{P}_{\text{real}}$) is related to the detected photon number probabilities ($\vec{P}_{\text{det}}$) by

$$\vec{P}_{\text{det}} = \mathbf{M}_{\text{XT}} \times \mathbf{M}_{\text{DC}} \times \mathbf{M}_{\text{FS}} \times \mathbf{M}_{\text{loss}} \times \vec{P}_{\text{real}}, \tag{5}$$

where $\mathbf{M}_{\text{XT}}, \mathbf{M}_{\text{DC}}, \mathbf{M}_{\text{FS}}, \mathbf{M}_{\text{loss}}$ are matrices quantifying the cross-talk, dark-counts, finite-size, and loss effects, respectively. The ordering of the loss and finite-size matrices is important here, but we do not show a proof of the correct ordering here. Instead, we observe that Eq. (5) agrees with previous theoretical results that do not take matrix ordering into account [9,25].

We first calculate the detected statistics for an n-photon Fock state, a state with a fixed number of n photons; then the result can be generalized to any other state by averaging over the real photon statistics. The probability for s detection events to occur due to an incident n-photon Fock state after accounting for all the distorting effects is

$$P^{n}_{\mathrm{det}}(s|\eta,d,N,\tilde{x}) = \sum_{p=0}^{s}\binom{p}{s-p}\left[\tilde{x}\left(1-\frac{p}{N}\right)\right]^{s-p}\left[1-\tilde{x}\left(1-\frac{p}{N}\right)\right]^{2p-s} \times \binom{N}{p}\sum_{j=0}^{p}\binom{p}{j}(-1)^{p-j}(1-d)^{N-j}\left(1-\eta+\frac{j\eta}{N}\right)^{n}. \tag{6}$$

This result is proven in Appendix A and agrees with previous analytical results substituting $\tilde{x}=0, d=0$ [25] and $\eta=1$ [9]. The agreement between the results shows that the loss should be operated before the finite-size effect as mentioned above.

The matrix $\Pi_{s,n} = P^{n}_{\mathrm{det}}(s|\eta,d,N,\tilde{x})$ is related to the positive operator-valued measure (POVM) of the detector, Π_s, by $\Pi_s = \sum_n \Pi_{s,n}|s\rangle\langle s|$ [31], where $|s\rangle$ represents an s-photon Fock state. Here, $\Pi_{s,n}$ is written using four parameters while in the POVM description the number of parameters is as the number of the matrix elements which usually is much greater than four. The implication is that more parameters are needed to be found experimentally. On the other hand, the POVM description does not assume anything about the detection process as has been done here.

III. EXPERIMENTAL SETUP FOR SPD CALIBRATION

The experimental setup is described in Fig. 1. Squeezed light is generated by a spontaneous parametric down-conversion (SPDC) process [21] from a 2-mm-thick β-BaB_2O_4 (BBO) crystal using a 390-nm doubled Ti:Sapphire pulsed laser. In the first part, a collinear type-I SPDC is used to generate a horizontally polarized SMSV state. And in the second part, a non-collinear type-II SPDC is used to generate a TMSV state. The two modes are set in orthogonal polarization modes, and spatially overlapped by a polarizing beam splitter (PBS). Then, the SV light is filtered spectrally by a 3-nm bandpass filter (BPF) and spatially by a single mode fiber (SMF), and attenuated by an adjustable neutral density filter (NDF). The attenuated light is directed to the detector under test (DUT). We note that a calibrated NDF is used as a convenient method for a known attenuation. Any other self-calibrated attenuation method can be used; for instance, the attenuation of SMSV can be applied by a single rotating polarizer.

From this point we focus on a single SPD, i.e., for $N=1$. In this case, there are only two possibilities; there is either a detection event or not. Mathematically it means $s=0$ or 1 in Eq. (6), and thus the cross-talk summation vanishes.

To calibrate an SPD, we have used both attenuated SMSV and TMSV states. Although only one of these states can be used, we show that both schemes will work for calibration purposes. It is convenient to define the odds $O^{\mathrm{n}}_{\mathrm{det}}(\eta,d,1,0) \equiv \frac{P^{\mathrm{n}}_{\mathrm{det}}(s=1|\eta,d,1,0)}{P^{\mathrm{n}}_{\mathrm{det}}(s=0|\eta,d,1,0)}$ of a detection event. We also replace $\eta \to \eta t$, where t is the transmission of the NDF, and henceforth η is the fixed efficiency and t is a variable. Following these changes, Eq. (6) is now reduced to

$$O^{\mathrm{SMSV}}_{\mathrm{det}}(\eta t,d,1,0) = \left(\frac{\sqrt{1+(2-\eta t)\eta\bar{n}t}}{1-d}-1\right) \approx \frac{\left(1-\frac{\eta t}{2}\right)\eta\bar{n}t+d}{1-d}, \tag{7}$$

$$O^{\mathrm{TMSV}}_{\mathrm{det}}(\eta t,d,1,0) = \frac{\left(1-\frac{\eta t}{2}\right)\eta\bar{n}t+d}{1-d}. \tag{8}$$

Here Eqs. (7) and (8) are for SMSV and TMSV states, respectively. The approximation is the Taylor expansion for $\bar{n} \ll 1$ and the full derivation is found in Appendix C.

Experimentally, the probability of detection is given by the ratio of the number of single counts (or detection events) to the number of pump pulses. This probability is measured while varying the transmission of the NDF. The efficiency parameter is then extracted from a second-order fit to Eq. (7) or Eq. (8). Multiplexed PNRs can also be calibrated in a similar manner, though we do not demonstrate it in this paper.

For comparison, the detection efficiency is also measured by the coincidence method by adding another SPD (denoted by "ref" in Fig. 1). For clarity, the beam path to the reference detector is indicated by a dashed line. For the TMSV setup a half-wave plate (HWP) is added, flipping the photon polarization to vertical polarization. After the PBS the photons propagate to different detectors as both photons are vertically

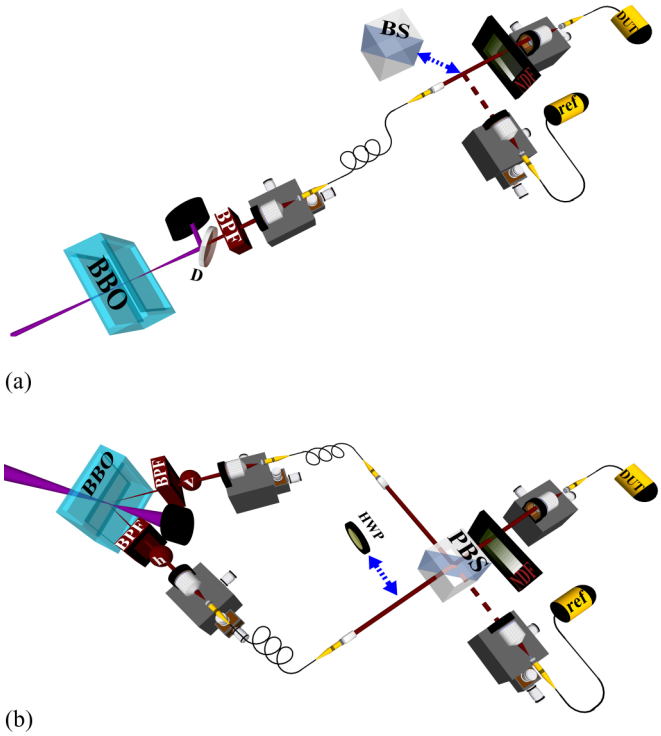

FIG. 1. The experimental setup for (a) SMSV state and (b) TMSV state. DM - dichroic mirror, PBS - polarizing beam splitter, BS - beam splitter, HWP - half wave-plate, BPF - bandpass filter, NDF - adjustable neutral density filter, DUT - detector under test. Note that the detector denoted as "ref" is only for comparison to the coincidence calibration procedure. See Fig. 4 and text for more details.

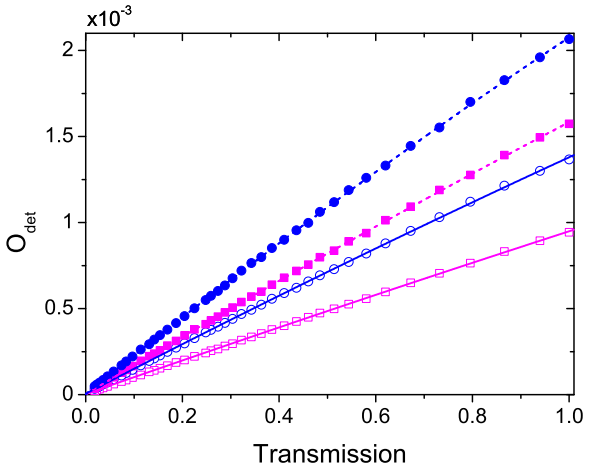

FIG. 2. The odds of a detection event as a function of the NDF transmission for two separate detectors. Solid and empty symbols denote data from using TMSV and SMSV, respectively. Solid and dashed lines are fits to Eqs. (7) and (8), respectively. SPD #1 is represented in blue circles and SPD #2 is represented in pink boxes. Error bars are assumed to be due to Poissonian noise and intensity fluctuations (see Fig. 6). The maximal error bar is 2.1×10^{-5} and is smaller than the symbol size; 3.3×10^{-5}, and thus not displayed.

polarized. For the SMSV setup a beamsplitter (BS) is added, such that half of the time the photons are split to both detectors, enabling to calibrate with the coincidence method. After the BS the probability for detection is $p_i = \frac{\tilde{p}}{4}(4\eta_i - \eta_i^2)$, where $i = a,b$ denotes the different SPDs, $\tilde{p}$ is the probability to generate a pair, and $p_{\text{coin}} = \frac{\tilde{p}}{2}\eta_a\eta_b$ is the probability for coincidence. Using the experimental results of p_a, p_b, and p_{coin} the efficiency is $\eta_a = 2\frac{p_{\text{coin}}}{p_b}\frac{1-\frac{1}{2}\frac{p_{\text{coin}}}{p_a}}{1-\frac{1}{4}\frac{p_{\text{coin}}}{p_a}\frac{p_{\text{coin}}}{p_b}} \approx 2\frac{p_{\text{coin}}}{p_b}$, and the expression for η_b is found by flipping a and b.

IV. EXPERIMENTAL RESULTS

The presented scheme is useful for evaluating the detection efficiency of an SPD due to the unique photon statistics of the SV light and the nonlinear loss, i.e., the inability of an SPD to detect more than one photon. The nonlinear loss alters the linear dependency of the single counts on the attenuation and the detection efficiency is extracted from the curvature.

The SPD counts were accumulated for one second for a range of 29 different attenuation values of the NDF. The probability for a photon detection is measured by the single counts divided by the total number of experiment runs. We repeat the experiment for two separate SPDs using both SMSV and TMSV to demonstrate the ability to calibrate detectors of different efficiency. The results are presented in Fig. 2. In each of the four measurements the data is fit to a second-order polynomial, i.e., $a_2t^2 + a_1t + a_0$. According to Eqs. (7) and (8) the efficiency is $\eta = -2\frac{a_2}{a_1}$.

In Table I, the results for the efficiency calibration by the presented method are summarized. Those results are compared to the coincidence method showing good agreement between the two methods, for all used detectors and for both experimental setups. The measured efficiency is the total efficiency of the setup, including in particular the detection efficiency of the detector and the coupling efficiency. The total efficiency is $\eta_T = \eta_d\eta_s$, where η_d is the detection efficiency of the detector, and η_s is the overall transmission of the system. For convenience, in the rest of the paper the T is omitted, i.e., $\eta \equiv \eta_T$. Here the total efficiency is presented and discussed, and the other efficiencies are presented in Appendix C. The coupling efficiency is lower in the SMSV setup due to weaker coupling to single-mode fiber, which is probably caused by spatial walk-off inside the nonlinear crystal. This inefficient coupling is a loss factor well observed by both calibration methods.

TABLE I. The efficiencies measured by the presented single detector method (η_1) and the two detector coincidence method (η_2). Note that the SMSV efficiencies are lower than in the TMSV case due to weaker coupling into the single-mode fiber.

SPD #	SV light	η_1	η_2
1	SMSV	$11.3 \pm 1.1\%$	$11.8 \pm 0.9\%$
2	SMSV	$7.4 \pm 0.9\%$	$8.1 \pm 0.9\%$
1	TMSV	$17.4 \pm 1.0\%$	$17.3 \pm 0.8\%$
2	TMSV	$12.7 \pm 0.9\%$	$11.7 \pm 0.8\%$

The method also predicts accurately the dark count probability. According to Eqs. (7) and (8) the dark count probability equals approximately to the zero order coefficient (denoted above by a_0). As before to get the number of dark counts per second, the probability is multiplied by the number of laser cycles per second. Doing that, we get 320 ± 40 dark counts per second for SPD #1 and 260 ± 30 for SPD #2. The dark count rates are well fit for measurements by directly counting the number of single detection events per second while covering the detector.

To show the presented method is valid for any pump power, we repeated the experiment using TMSV and SPD #1 for different pump powers of the up-converted beam. The results of this process are shown in Fig. 3. As before, we fit the measurements to a second-order polynomial and the efficiency is calculated from the polynomial coefficients.

The results for different pump powers are summarized in Table II. A good agreement is shown between different pump powers, where a standard deviation of 0.5% is found. The standard deviation is consistent with the error values of the detection efficiency which were calculated separately.

The presented method can also work with a much stronger pump power where the squeezed light contains more than two photons with substantial probability. As opposed to the coincidence method where high photon numbers distort the

TABLE II. The efficiencies as measured by the presented method (η_1) with SPD #1 and TMSV light for different pump powers.

Pump power	η_1
145 mW	$17.9 \pm 0.8\%$
180 mW	$16.5 \pm 0.9\%$
215 mW	$17.2 \pm 0.8\%$
240 mW	$16.8 \pm 0.7\%$
250 mW	$17.6 \pm 0.7\%$

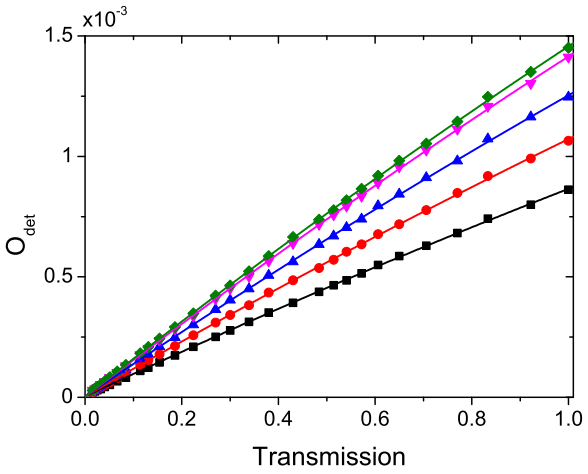

FIG. 3. The odds of a detection event as a function of the NDF transmission for SPD #1 when the pump power is varied. Green diamonds are for pump power of 250 mW, pink downward triangles for 240 mW, blue triangles for 215 mW, red circles for 180 mW, and black boxes for 145 mW. Error bars are assumed to be due to Poissonian noise and intensity fluctuations (see Fig. 6). The maximal error bar is 2.1×10^{-5} and is smaller than the symbol size; 3.3×10^{-5}, and thus not displayed.

result for the detection efficiency, our method takes into account all the photon statistics including probabilities for high photon numbers, and thus, can only be improved by the higher signal-to-noise ratio.

The method incorporates squeezed light as its statistics enables calibration. Yet, there might be better light sources for calibration, but this optimization is left for future works. Nevertheless, coherent states and thermal states (one mode of TMSV) had been checked both theoretically and experimentally and the results of the odds (O^{n}_{det}) showed no dependence on the SPD efficiency.

The dead time of the detectors has a minor influence on the results. Assuming a random process, the distribution of pulse difference between consecutive events is $P(n) = p \times (1-p)^{n-1}, n = 1 \ldots \infty$, where p is the probability for detection event per pump pulse (assuming zero dead time). In our system the laser cycle is 13 ns and the dead time is 50 ns. Thus, the probability to miss an event due to the detector dead time is $\sum_{n=1}^{3} P(n) = 1-(1-p)^3 \approx 3p$. The maximal probability for an event is $p \sim 10^{-3}$, which means that the correction of the dead time effect is less than one percent and comparable to the experimental error.

If this effect is not negligible, it is another factor for the nonlinear loss. Thus, this nonlinear loss would result in measuring falsely higher detection efficiencies. As mentioned in Sec. IV, the presented method uses the nonlinear loss of multiple photon detection, assuming a single nonlinear loss effect. The nonlinear loss causes the single photon counts to deviate from a linear curve. This deviation enables to measure the efficiency as $\eta = -2\frac{a_2}{a_1}$. During the dead time period, the detector cannot detect new photons. Its efficiency in this stage is actually zero. Thus, the larger the photon flux, the larger the chance that more photons will not be detected, resulting in a larger nonlinear response that is falsely translated by the fit to a larger detected efficiency. This upward deviation of the measured efficiency is larger for greater pump powers as the photon flux is greater. Thus, the measured efficiency should increase when the pump power increases, but Table II shows no such dependence and therefore the dead time effect on our results is negligible. Reducing the experimental errors and observing this deviation will enable to measure the dead time of the detector.

If a continuous wave (CW) laser would be used, the distribution of time difference between consecutive events is $P(t) = \frac{1}{t_0}e^{-t/t_0}$, where t_0 is the average time between consecutive events. Then, the probability to miss an event due to detector dead time is $\int_0^{\tau}\frac{1}{t_0}e^{-t/t_0}dt = 1-e^{-\tau/t_0}$, where τ is the dead time of the detector. Thus, also for CW laser the influence of the dead time is negligible if $\frac{\tau}{t_0}$ is small, and anyway can be corrected.

V. SUMMARY

To summarize, we present a model to characterize a PNR detector based on SPDs. This model predicts the detected photon statistics in the presence of loss, finite size, dark counts, and cross-talk. The model is valid also for a single SPD. As an application for the model, we show that the detection efficiency can be found by measuring the single counts without coincidence counts, i.e., without a reference detector. We experimentally measure the efficiency of two different SPD detectors and successfully compare it to the coincidence method.

APPENDIX A: PROBABILITY CALCULATION

We first replace the matrix products in Eq. (5) into summations and substitute the matrix values according to Eqs. (1) to (4):

$$\begin{aligned} &P^{n}_{\mathrm{det}}(s|\eta,d,N,\tilde{x}) \\ &= \sum_{p=0}^{N}\binom{p}{s-p}\left[\tilde{x}\left(1-\frac{p}{N}\right)\right]^{s-p}\left[1-\tilde{x}\left(1-\frac{p}{N}\right)\right]^{2p-s} \\ &\times \sum_{k=0}^{N}\binom{N-k}{p-k}d^{p-k}(1-d)^{N-p} \\ &\times \sum_{m=0}^{N}\frac{1}{N^m}\binom{N}{k}k!S(m,k)\binom{n}{m}\eta^m(1-\eta)^{n-m}. \end{aligned} \tag{A1}$$

Now, we focus on the two last lines in Eq. (A1). We notice that $m \leqslant n$ and $k \leqslant p$ because the loss effect cannot increase the photon number and dark-counts cannot decrease it. After reordering the summations and substituting $\binom{N}{k}\binom{N-k}{p-k} = \binom{N}{p}\binom{p}{k}$ we get

$$\begin{aligned} &\binom{N}{p}\sum_{m=0}^{n}\frac{1}{N^m}\binom{n}{m}\eta^m(1-\eta)^{n-m} \\ &\times \sum_{k=0}^{p}\binom{p}{k}d^{p-k}(1-d)^{N-p}\sum_{j=0}^{k}(-1)^{k-j}\binom{k}{j}j^m. \end{aligned} \tag{A2}$$

We reorder the summations in the second line, use $\binom{p}{k}\binom{k}{j} = \binom{p}{j}\binom{p-j}{k-j}$ and replace the summation index $k \to k-j$, resulting in the second line to be

$$\sum_{j=0}^{p}\binom{p}{j}j^m\sum_{k=0}^{p-j}\binom{p-j}{k}(-1)^k d^{p-k-j}(1-d)^{N-p}. \quad \text{(A3)}$$

The inner summation equals to $(1-d)^{N-j}(-1)^{p-j}$. Substituting this in Eq. (A2) and reordering the summations, we get

$$\binom{N}{p}\sum_{j=0}^{p}\binom{p}{j}(1-d)^{N-j}(-1)^{p-j} \times \sum_{m=0}^{n}\binom{n}{m}\left(\frac{\eta j}{N}\right)^m(1-\eta)^{n-m}. \quad \text{(A4)}$$

However, the second summation is a binomial expansion and regrouping it restores the third line of Eq. (6). The second line remains almost as is. The upper limit is changed to s, the total number of activated elements, as p, the number of activated elements by signal photon and dark counts, is limited by s.

APPENDIX B: CALCULATING SPD PROBABILITIES FOR SV STATES

Substituting $N = 1$ in Eq. 6, i.e.,

$$P^n_{\text{det}}(s|\eta,d,1,\tilde{x}) = \sum_{j=0}^{p}\binom{p}{j}(-1)^{p-j}(1-d)^{1-j}(1-\eta+j\eta)^n. \quad \text{(B1)}$$

The first summation in Eq. (6) vanishes as an SPD has no neighbors to cross-talk to. We write the probabilities for no detection and for one photon detection explicitly

$$P^n_{\text{det}}(0|\eta,d,1,0) = (1-d)(1-\eta)^n, \quad \text{(B2)}$$

$$P^n_{\text{det}}(1|\eta,d,1,0) = 1-(1-d)(1-\eta)^n. \quad \text{(B3)}$$

The probability to have zero photon counts is just the probability to not detect n photons times the probability to not have dark-counts. The probability to get one photon detection is just the complementary probability. Next, we average over the photon statistics of the SV state.

For a TMSV state any mode has photon statistics of $P(n) = (1-x)x^n$ where x is related to $\bar{n}$, the average photon number, by $x = \frac{\bar{n}}{1+\bar{n}}$. After combining the two modes spatially the probability for $2n$-photons is $P_{\text{TMSV}}(2n) = (1-x)x^n$ [21]. We average on the statistics and get

$$P^{\text{TMSV}}_{\text{det}}(0|\eta,d,1,0) = \frac{(1-d)(1-x)}{1-x(1-\eta)^2}, \quad \text{(B4)}$$

$$P^{\text{TMSV}}_{\text{det}}(1|\eta,d,1,0) = 1-\frac{(1-d)(1-x)}{1-x(1-\eta)^2}. \quad \text{(B5)}$$

Taking the ratio of the two last equations gives Eq. (8).

For a SMSV state the photon statistics is $P_{\text{SMSV}}(n) = \cos^2\frac{n\pi}{2}\frac{n!}{2^n[(\frac{n}{2})!]^2}\frac{\tanh r^n}{\cosh r}$, where r is the squeezed parameter [21].

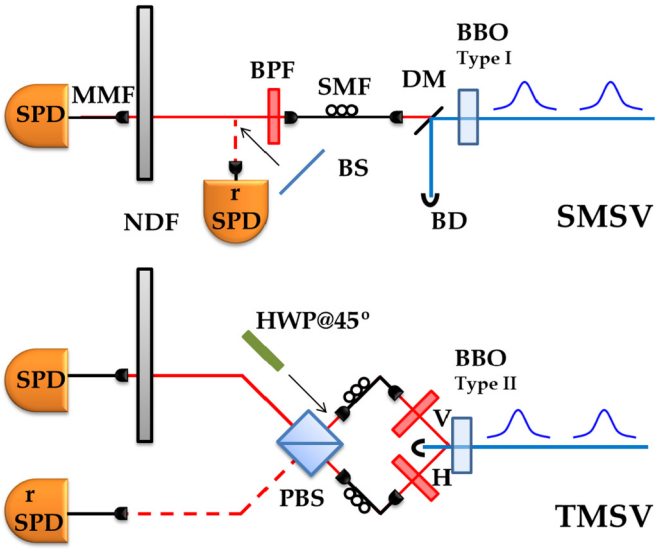

FIG. 4. Detailed experimental setup. DM: dichroic mirror, PBS: polarizing beam splitter, BS: beam splitter, HWP: half wave-plate, BPF: bandpass filter, NDF: adjustable neutral density filter, DUT: detector under test, SMF: single-mode fiber, MMF: multimode fiber, BD: beam dump.

After the averaging we get

$$P^{\text{SMSV}}_{\text{det}}(0|\eta,d,1,0) = (1-d)\frac{1}{\sqrt{1+(2\eta-\eta^2)\bar{n}}}, \quad \text{(B6)}$$

$$P^{\text{SMSV}}_{\text{det}}(1|\eta,d,1,0) = 1-(1-d)\frac{1}{\sqrt{1+(2\eta-\eta^2)\bar{n}}}, \quad \text{(B7)}$$

where $\bar{n} = \sinh^2 r$ is the average photon number and the hyperbolic function identities, $\cosh(\tanh^{-1} r) = \frac{1}{\sqrt{1-r^2}}$, $\cosh^2 r - \sinh^2 r = 1$, were used. Taking the ratio of the two last equations yields Eq. (7).

APPENDIX C: DETAILED EXPERIMENTAL SETUP

Figure 4 shows the experimental setup with additional technical details. A 150-fs pulsed Ti:Sapphire laser (MIRA 900 Coherent) with a 76-MHz repetition rate is frequency doubled to a wavelength of 390 nm (not shown). The up-converted beam is focused on a 2-mm-thick β-BaB_2O_4 (BBO) crystal. More than 99% of the up-converted beam is filtered by a dichroic mirror (DM) for the collinear setup (SMSV) or spatially for the noncollinear setup (TMSV). The remaining pump photons are

TABLE III. The detection efficiency η_d, the transmission of the optics, T_O, the coupling efficiency η_c, the overall transmission of the system $\eta_s = T_O\,\eta_c$, and the efficiency measured by the single detector method $\eta_1 = \eta_s\eta_d$.

SPD #	SV light	η_d	η_s	T_O	η_c	η_1
1	SMSV	$60\pm5\%$	$16\pm2\%$	$\sim80\%$	$20\pm3\%$	$11.3\pm1.1\%$
2	SMSV	$60\pm5\%$	$16\pm2\%$	$\sim80\%$	$20\pm3\%$	$7.4\pm0.9\%$
1	TMSV	$60\pm5\%$	$24\pm3\%$	$\sim80\%$	$30\pm4\%$	$17.4\pm1.0\%$
2	TMSV	$60\pm5\%$	$24\pm3\%$	$\sim80\%$	$30\pm4\%$	$12.7\pm0.9\%$

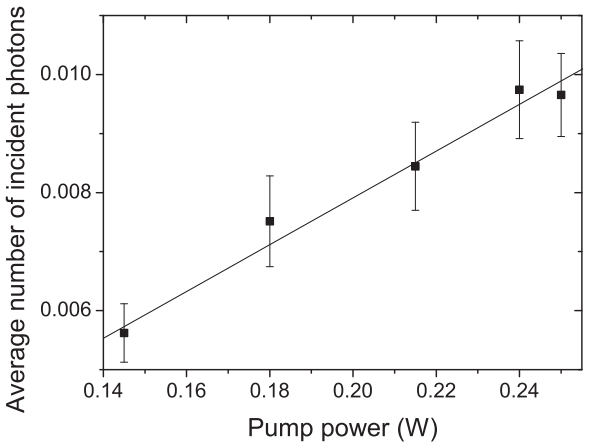

FIG. 5. The average number of incident photons as a function of the pump power.

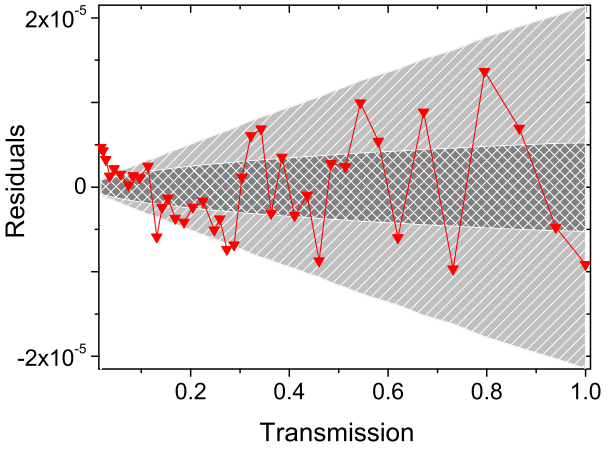

FIG. 6. Residuals and error calculation for TMSV SPD #1 (see Fig 2).

unguided by the fibers. We verified prior to the experimental measurements, that no pump photons arrive at the detector. Single-mode filtration is done by 3-nm width bandpass filter (BPF) centered around 780 nm, and a step index 5 μm core single mode fiber (SMF). The TMSV is given by single spatial and spectral modes and two polarization modes, spatially overlapped using a polarizing beam splitter (PBS). The signal beam is directed to a (variable) neutral density filter (NDF) and recollected with a graded index 62.5 μm core multimode fiber (MMF) with collection efficiency of more than 90%. The detector under test (DUT) is an avalanche photodiode single-photon detector (SPD) (Perkin Elmer SPCM-AQ4C). A reference detector (ref SPD) is used for comparison with the coincidence method, where we added a beam splitter (BS) and a half-wave plate (HWP) to split the photons into both detectors.

The efficiencies and the transmission of the optics are summarized in Table III. The SPDs, used in the experiment, have efficiency of 55–65%, thus, the transmission of the system is $24 \pm 3\%$ for TMSV and $16 \pm 2\%$ for SMSV. The transmission of the bandpass filters is estimated to be around 90% and the rest of the optics also around 90%, thus the fiber coupling efficiency is $30 \pm 4\%$ and $20 \pm 3\%$ for the TMSV and SMSV, respectively.

APPENDIX D: EXTRACT THE AVERAGE PHOTON NUMBERS

Figure 5 shows the linear relation of the pump power and the average number of incident photons. The average number of incident photons,$\bar{n}$, is calculated by $\bar{n} = -\frac{1}{2}\frac{a_1^2}{a_2}$ where a_2, a_1 are the polynomial coefficients of the fit to Eq. (8) (as in the text). As expected, the fit has a linear dependence, where 0.04 photons per watt, on average, are generated.

APPENDIX E: ERROR CALCULATION

Error ranges and residuals are plotted in Fig. 6. The data points are the residuals of the experimental data. The red line is for guiding the eye. The dark-gray checkered area denotes the Poissonian error range. The Poissonian error only partially explains the residual. After adding a fixed error of 1% due to intensity fluctuation (light-gray dashed area), the residuals are contained within the error range.

[1] E. Knill, R. Laflamme, and G. J. Milburn, Nature (London) **409**, 46 (2001).

[2] P. Kok, W. J. Munro, K. Nemoto, T. C. Ralph, J. P. Dowling, and G. J. Milburn, Rev. Mod. Phys. **79**, 135 (2007).

[3] L. Cohen, D. Istrati, L. Dovrat, and H. S. Eisenberg, Opt. Exp. **22**, 11945 (2014).

[4] Y. Israel, S. Rosen, and Y. Silberberg, Phys. Rev. Lett. **112**, 103604 (2014).

[5] C. C. Gerry, J. Mimih, and A. Benmoussa, Phys. Rev. A **80**, 022111 (2009).

[6] T. Horikiri and T. Kobayashi, Phys. Rev. A **73**, 032331 (2006).

[7] R. H. Hadfield, Nat. Photon. **3**, 696 (2009).

[8] B. Dolgoshein *et al.*, Nucl. Instrum. Methods **563**, 368 (2006).

[9] M. J. Fitch, B. C. Jacobs, T. B. Pittman, and J. D. Franson, Phys. Rev. A **68**, 043814 (2003).

[10] A. Migdall, S. V. Polyakov, J. Fan, and F. C. Bienfang, *Single-Photon Generation and Detection: Physics and Applications*, Vol. 45, (Academic, New York, 2013).

[11] D. N. Klyshko, Sov. J. Quantum Electron. **7**, 591 (1977).

[12] G. K. Kitaeva, A. N. Penin, V. V. Fadeev, and Y. A. Yanait, Sov. Phys. Dokl. **24**, 564 (1979).

[13] J. Peřina, Jr., O. Haderka, A. Allevi, and M. Bondani, Appl. Phys. Lett. **104**, 041113 (2014).

[14] A. P. Worsley, H. B. Coldenstrodt-Ronge, J. S. Lundeen, P. J. Mosley, B. J. Smith, G. Puentes, N. Thomas-Peter, and I. A. Walmsley, Opt. Exp. **17**, 4397 (2009).

[15] A. Avella, G. Brida, I. P. Degiovanni, M. Genovese, M. Gramegna, L. Lolli, E. Monticone, C. Portesi, M. Rajteri, M. L. Rastello, E. Taralli, P. Traina, and M. White, Opt. Exp. **19**, 23249 (2011).

[16] M. Bohmann, R. Kruse, J. Sperling, C. Silberhorn, and W. Vogel, Phys. Rev. A **95**, 033806 (2017).

[17] X.-H. Chen, Y.-H. Zhai, D. Zhang, and L.-A. Wu, Opt. Lett. **31**, 2441 (2006).

[18] A. Czitrovszky, A. V. Sergienko, P. Jani, and A. Nagy, Metrologia **37**, 617 (2000).

[19] M. López, H. Hofer, and S. Kück, J. Mod. Opt. **62**, 1732 (2015).

[20] M. A. Wayne *et al.*, Opt. Exp. **25**, 20352 (2017).

[21] C. C. Gerry and P. L. Knight, *Introductory Quantum Optics* (Cambridge University Press, Cambridge, England, 2005), Secs. 7.1, 7.3, and 7.7.

[22] L. Dovrat, M. Bakstein, D. Istrati, A. Shaham, and H. S. Eisenberg, Opt. Exp. **20**, 2266 (2010).

[23] L. Dovrat, M. Bakstein, D. Istrati, and H. S. Eisenberg, Phys. Scr. **T147**, 014010 (2012).

[24] B. E. A. Saleh and M. C. Teich, *Fundamentals of Photonics* (Wiley, New York, 1991).

[25] H. Paul, P. Törmä, T. Kiss, and I. Jex, Phys. Rev. Lett. **76**, 2464 (1996).

[26] E. W. Weisstein, triangle **7**, 8 (2002).

[27] P. Buzhan, B. Dolgoshein, L. Filatov, A. Ilyin, V. Kaplin, A. Karakash, S. Klemin, R. Mirzoyan, A. Otte, E. Popova, V. Sosnovtsev, and M. Teshima, Nucl. Instrum. Methods **567**, 78 (2006).

[28] I. Afek, A. Natan, O. Ambar, and Y. Silberberg, Phys. Rev. A **79**, 043830 (2009).

[29] M. Akiba, K. Tsujino, K. Sato, and M. Sasaki, Opt. Exp. **17**, 16885 (2009).

[30] P. Eraerds, M. Legré, A. Rochas, H. Zbinden, and N. Gisin, Opt. Exp. **15**, 14539 (2007).

[31] G. Brida, L. Ciavarella, I. P. Degiovanni, M. Genovese, A. Migdall, M. G. Mingolla, M. G. A. Paris, F. Piacentini, and S. V. Polyakov, Phys. Rev. Lett. **108**, 253601 (2012).